



HAL
open science

Kinetic modelling of individual starch granules swelling

Arnesh Palanisamy, François Deslandes, Marco Ramaioli, Paul Menut,
Artemio Plana-Fattori, Denis Flick

► **To cite this version:**

Arnesh Palanisamy, François Deslandes, Marco Ramaioli, Paul Menut, Artemio Plana-Fattori, et al.. Kinetic modelling of individual starch granules swelling. *Food Structure*, 2020, 26, pp.10150. 10.1016/j.foostr.2020.100150 . hal-02934941

HAL Id: hal-02934941

<https://hal.science/hal-02934941>

Submitted on 14 Sep 2020

HAL is a multi-disciplinary open access archive for the deposit and dissemination of scientific research documents, whether they are published or not. The documents may come from teaching and research institutions in France or abroad, or from public or private research centers.

L'archive ouverte pluridisciplinaire **HAL**, est destinée au dépôt et à la diffusion de documents scientifiques de niveau recherche, publiés ou non, émanant des établissements d'enseignement et de recherche français ou étrangers, des laboratoires publics ou privés.

Kinetic Modelling of Individual Starch Granules Swelling

Arnesh Palanisamy^a, François Deslandes^b, Marco Ramaioli^a, Paul Menut^a, Artemio Plana-Fattori^a, Denis Flick^{a,*}

^a *Université Paris Saclay, INRAE, AgroParisTech, UMR SayFood, 91300, Massy, France*

^b *Université Paris Saclay, INRAE, AgroParisTech, UMR MaIAGE, 78350, Jouy-en-Josas, France*

Abstract

A novel kinetic model is proposed for individual starch granule swelling based on swelling kinetics time series data. The data was acquired from time-lapse microscopy observations of starch granules in a dilute suspension and subsequent image analysis. Chemically modified waxy-maize starch was used. The size evolution of many granules when subjected to various hydro-thermal treatments on a temperature-controlled stage was determined. Observations showed that swelling is not an instantaneous process and varies from a granule to another. A model has been developed which takes into account the effect of temperature evolution and variability between the granules on their swelling. This model can contribute to robust multi-scale simulation of industrial processes involving starch suspensions.

Keywords: Starch Granule, Image analysis, Swelling kinetics, Time-series data, Modelling

1. Introduction

Starch is the predominant food reserve in plants and provides 70-80% of the calories consumed by humans worldwide in various forms of food products (Bertolini, 2010). In 2000, the world starch production was estimated to be around 48.5 million tons, including native and modified starches. Hence, starch has been a perennial subject of research through decades. Starch granules majorly consists of two polymers: amylose and amylopectin. Both amylose and amylopectin have α -glucose as the monomer, however, their difference arises

*corresponding author

Email address: denis.flick@agroparistech.fr (Denis Flick)

8 from their linkages. Amylose has $\alpha(1-4)$ and is linear whereas amylopectin has $\alpha(1-6)$ and is
9 highly branched. The ratio of amylose and amylopectin in the starch granule depends on its
10 source and botanical origin. This in turn has drastic consequences on the physical properties
11 such as rheology (Banks et al., 1974; Hoover, 2001; Srichuwong et al., 2005; Visser et al.,
12 1997). Molecular properties such as molecular weight distribution and degree of amylopectin
13 branching are also known to impact the functional attributes at the macro-scale (Blennow
14 et al., 2001; Fredriksson et al., 1998; Singh et al., 2007).

15 Gelatinization is the process in which starch granules undergo an irreversible transforma-
16 tion when subjected to thermomechanical treatment in the presence of water. During this
17 process starch granules swell by imbibing water and increase the overall viscosity of the sus-
18 pension. It is also sometimes referred to as starch pasting in literature. Starch granules are
19 semi-crystalline with concentric rings of crystalline and amorphous phases (Ratnayake and
20 Jackson, 2008). On the microscopic scale, the process corresponds to the melting of crys-
21 tallites, loss of birefringence, leaching of amylose into the continuous phase and sometimes
22 rupture of the granular structure (Atwell, 1988; Biliarderis, 1992). During gelatinization,
23 melting of crystalline region in the granule occurs and depending on the origin of the starch,
24 the range for this transition is between 60 and 70 °C (Slade and Levine, 1995). The evolu-
25 tion of viscosity during gelatinization is also influenced by the process parameters such as
26 concentration, shear rate, thermal history, pH and presence of other ingredients (Thomas
27 and Atwell, 1999; Malumba et al., 2018). For high amylopectin cereal starches such as waxy
28 maize starch, the granules tend to hydrate with ease, swell rapidly and rupture to a great
29 extent which results in loss of paste viscosity. The rupture of the granules can be avoided
30 by chemically modifying the starch. This involves cross-linking via chemical bonds that act
31 as bridges between the two macromolecules. The introduction of functional groups into the
32 starch molecules such as acetylation results in lower amylose leaching properties of starch.
33 The resulting modified starches have markedly altered physicochemical properties (Ashog-
34 bon and Akintayo, 2014). Waxy maize starch is used in a wide variety of applications in the
35 food industry owing to its stability (Tattiyakul and Rao, 2000).

36 The sensory perception of viscosity is an important mouthfeel sensation (Szczesniak,

37 1963; Wood, 1968). Starch is used as a viscosity enhancer in many food formulations.
38 Hence, it is critical to accurately predict viscosity changes both from a product development
39 standpoint and an engineering design standpoint. During the thermal processing of liquid
40 food product containing starch, viscosity changes must be known to accurately estimate
41 process variables as the process is highly coupled in terms of heat transfer, momentum
42 transfer and transformation (Plana-Fattori et al., 2016). This warranted decades of research
43 into the sole aspect of viscosity predictions and significant literature exist regarding the chief
44 aspects which dictate the same. They are (a) the suspending medium's viscosity η_0 , (b) the
45 granule's volume fraction ϕ , (c) the granule's deformability, and (d) the imposed shear rate
46 (Chen et al., 2007). Nayouf et al. (2003) indicated that volume fraction of granules can be
47 estimated if the mean granule size (D_t) can be accurately determined.

48 Increasingly researchers started defining progress of gelatinization in terms of the increase
49 in diameter of granules (Anuntagool et al., 2017; Okechukwu and Rao, 1996; Bagley and
50 Christianson, 1982; Bakshi and Singh, 1980; Suzuki et al., 1976; Doublier et al., 1987; Kokini
51 et al., 1992). Alternate methods used to define gelatinization are based on DSC, rheology or
52 birefringence (Cui et al., 2014; Choi and Kerr, 2004; Dolan and Steffe, 1990; Biliaderis and
53 Prokopowich, 1994; Chang and Liu, 1991; I'anson et al., 1990; Kohyama and Nishinari, 1991;
54 Miles et al., 1985; Slade and Levine, 1991). However these are all equivalent indications of
55 the same process. Granule swelling occurs in two phases, first is the hydration phase where
56 there is a slight reversible increase in the diameter of the granules typically occurring in the
57 temperature range 30–60 °C and a second irreversible phase where there is a large increase
58 in diameter occurring at temperatures above 60 °C (Okechukwu and Rao, 1996). Some
59 authors reported that mean size and size distribution of swollen granules were correlated
60 with suspension consistency and flow behavior index (Okechukwu and Rao, 1996; Steeneken,
61 1989; Evans and Lips, 1990). Thus, there have been multiple attempts at kinetic modelling
62 this phenomena to predict the particle size evolution.

63 Kubota et al. (1979) attempted to model this phenomena with Arrhenius law and pro-
64 posed a first order kinetic equation with respect to non-dimensionalised consistency index.
65 Okechukwu and Rao (1995) introduced a similar rate equation with another dimensionless

66 variable called extent of gelatinization based on mean particle diameter of the population.
67 Lagarrigue et al. (2008) used the same formulation but argued that the reaction is second
68 order. Krüger et al. (2003) proposed a kinetic model which suggest the rate of increase
69 in diameter is proportional to the inverse of the mean diameter of the population diame-
70 ter with Arrhenius behavior and reaching a plateau at maximum diameter. Some authors
71 also suggested a set of reactions to describe gelatinization (Kokini et al., 1992). Malumba
72 et al. (2013) compared a wide range of rate expressions (Nth order kinetic, Diffusional,
73 Phase boundary and Avrami-Erofeev) to predict the isothermal swelling kinetics at different
74 temperatures and showed that the predictability was best for Nth order reaction models
75 especially second order and third order. They concluded that starch granule gelatinization
76 is not a simple water diffusion or a boundary phenomenon. The heat transferred inside the
77 granules induces phenomena such as melting of the crystallite, interaction between carbo-
78 hydrate polymers. This includes inter-chain and intra-chain polymer folding and hydrogen
79 bonding proceeding with semi-cooperative swelling of granules. They also argued that acti-
80 vation energy reported in literature must be called apparent activation energy as the same,
81 changed based on the form and order of the rate equation assumed. Plana-Fattori et al.
82 (2016) have used a modified form of rate constant with a cutoff minimum temperature
83 instead of the traditional Arrhenius form, which they substantiated with experiments.

84 All the above-mentioned works have always been attempts to model the swelling kinetics
85 of the population mean but not at the individual granule scale. Desam et al. (2018) tried to
86 model the swelling of a single granule based on diffusion kinetics and Flory-Huggins theory
87 of polymer mixing, but the model assumes all granules to have similar cross-links, tortu-
88 osity, and elastic restoring force. In this work, we propose a novel kinetic modeling at the
89 individual granule scale rather than the population mean. Time-series data obtained from
90 image processing of hot stage coupled microscope time-lapse images was used for building
91 and fitting the model. This model captures the inter granule variability of starch swelling
92 in water. This variability has not been quantified and addressed adequately in the previous
93 modeling works. We try to capture these nuances in this work albeit it empirically and
94 thus the parameters obtained are valid for chemically stabilized cross-linked waxy maize

95 starch (acetylated distarch adipate, C*Tex 06205), provided by Cargill (Baupte, France).
96 The method developed here enables modeling at the granular scale allowing one to capture
97 the dynamics better for multi-scale modeling translating into wide-reaching consequences
98 in plant equipment design, optimization, differentiated product development, simulation,
99 robust process development and robust model based process control systems.

100 **2. Materials and methods**

101 *2.1. Experimental method*

102 Chemically stabilized cross-linked waxy maize starch (C*Tex 06205), provided by Cargill
103 (Baupte, France), cross-linked via adipates, was used in $0.5g.kg^{-1}$ suspensions of starch in
104 water. This starch is composed of 99 % of amylopectin and less than 1% of amylose. This
105 type of starch does not lead to disruption and no release of amylose content is expected.
106 In terms of functionality, it has notably a good resistance to shear forces, a good storage
107 stability and a high paste clarity. The suspension was preheated to $50^{\circ}C$ under gentle
108 stirring with a magnetic pellet. Using a dropper sampling was performed and sample was
109 transferred to the microscopic glass slides with adhesive spacers of $250 \mu m$. Samples were
110 observed under 50X magnification using an Olympus BX-51 microscope (Olympus Optical
111 Co. Ltd., Tokyo, Japan). Images were acquired using a Basler A102fc digital camera (Basler
112 AG, Ahrensburg, Germany). Each observation is an 8 bit image of 1388×1038 pixels which
113 represents a $361 \times 270 \mu m^2$ area. Microscope glass slides with samples were placed on a
114 Linkam LTS120 stage (Linkam Scientific Instruments, Surrey, UK). The temperature was
115 controlled with the Linksys32 software. The samples were subjected to different temperature
116 profiles, starting with a holding at $50^{\circ}C$ for 1 min (figure 1a). Some samples were observed
117 under the microscope at different constant temperatures from $55^{\circ}C$ to $62^{\circ}C$ for 1 hour; no
118 image processing was carried out for these experiments as the objective of the same was only
119 to observe if the granules began to swell and to estimate the latency time before swelling.

120 *2.2. Image data analysis and notation*

121 The Java plugin for ImageJ software developed by Deslandes et al. (2019) was used to
 122 process the images. Ferret diameter is a length of an object measured along a specified
 123 direction. Thus, along different direction we have different Ferret lengths. We note the
 124 minimum and maximum Ferret diameter of a granule (μm), m and M respectively. The
 125 diameter of the granule is taken as the geometric mean of the Ferret lengths:

$$D = \sqrt{Mm}. \quad (1)$$

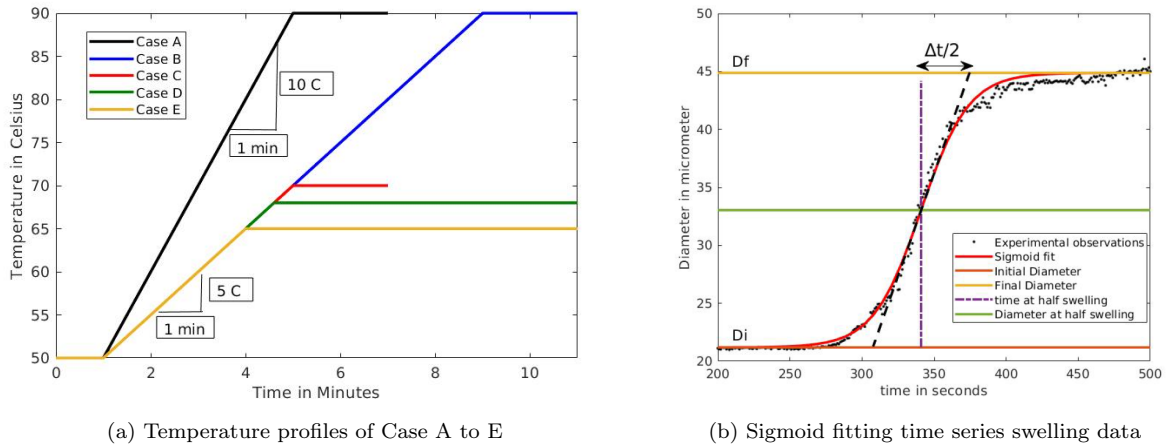


Figure 1

126 Image analysis and subsequent sigmoid curve fitting for the resulting time series data
 127 of diameter as a function of time was done following the procedure outlined in Deslandes
 128 et al. (2019). The parameters D_i , D_f , δ and $t_{1/2}$ denote the initial diameter (μm), the
 129 final diameter (μm), the swelling rate (s^{-1}) and the half-swelling time (s) of the granule
 130 respectively. These morphological and kinetics parameters are estimated by performing
 131 least-squares fitting on the size evolution data obtained from the image processing onto the
 132 sigmoid curve given by equation 2 (Deslandes et al., 2019). A typical diameter evolution of
 133 a granule with time along the least square fitting of the sigmoid curve is depicted in figure
 134 1b.

$$\tilde{D}(t) = \frac{D_f - D_i}{1 + e^{-\delta(t-t_{1/2})}} + D_i \quad (2)$$

135 The beginning of the 1 minute hold time at 50 °C is taken as the origin of time and
 136 different temperature profiles as depicted in the figure 1a are imposed on the sample. The
 137 individual granule swelling duration (Δt) is estimated by extrapolation of the tangent at the
 138 half-swelling time. It can be calculated from the parameter δ using the following equation:

$$\Delta t = \frac{4}{\delta}. \quad (3)$$

139 We then define t_{onset} , the individual swelling onset time by

$$t_{onset} = t_{1/2} - \frac{\Delta t}{2}. \quad (4)$$

140 3. Experimental results and observation

141 3.1. Observation at constant temperature between 55 °C and 62 °C

142 Observing the samples under the microscope at different constant temperatures starting
 143 from 55 °C to 62 °C for 1 hour was the objective to determine the minimum temperature at
 144 which swelling starts. It was observed as shown in images of figure 2, the gradual increase in
 145 fraction of granules swollen as temperature increases from 57 °C to 62 °C. We can safely say
 146 that it required at least around 60 °C to observe swelling in majority of the granules, this is
 147 consistent with the literature reported values (Slade and Levine, 1995). However, this may
 148 not be entirely true as we saw some granules swell at 58 °C and some granules not swollen
 149 at 62 °C even after a duration of 1 hour. Nevertheless, in industrial processes, the maximal
 150 temperature is always much greater than 70 °C and residence time in heat exchangers is of
 151 some minutes only. In light of the practicality and the relevance to the industrial process,
 152 we make this assumption that the minimum swelling temperature is of 60 °C for all the
 153 granules.

154 For the experiments carried for 1 hour (1 image per 5 seconds) at 62 °C, the latency time
 155 in the onset of swelling was manually noted from the diameter vs time data obtained after
 156 post processing using the plugin developed by Deslandes et al. (2019). Figure 3 shows the
 157 experimental cumulative distribution (47 granules) and an exponential curve fit for the same.

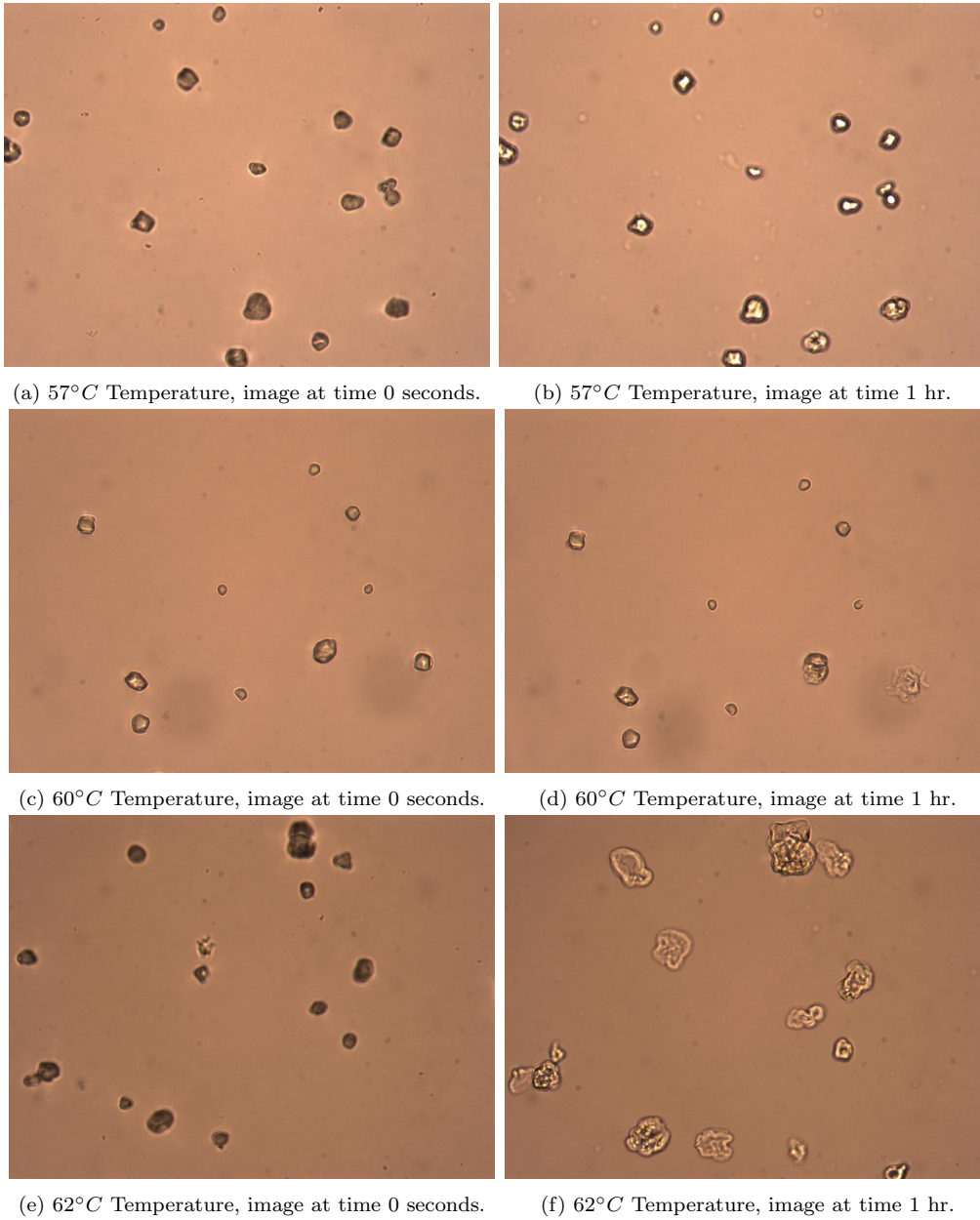


Figure 2: Starch granules at the beginning and after 1 hour at different temperatures

158 We use this information in the section 4.1 to justify the choice of mathematical formulation.

159 *3.2. Diameter increase during temperature ramp*

160 The results of the image processing and data analysis during different temperature ramps
 161 are summarized in the table 1. Note that for the case E with maximum temperature 65°C
 162 only the completely swollen granules were used to compute the sigmoid curve parameters.

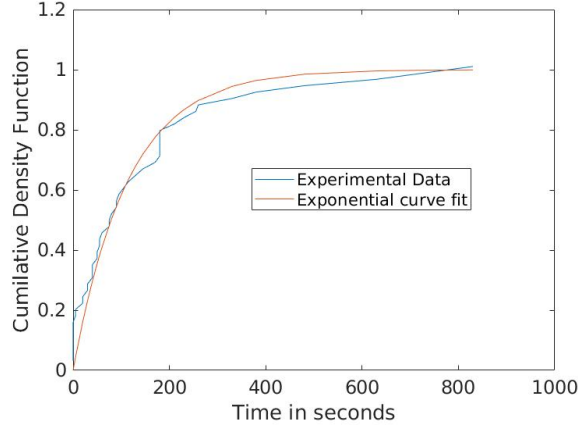


Figure 3: Experimental delay times for swelling onset at 62 °C

163 All the reported cases had a lapse rate of 1 image per second. The onset times reported
 164 here are from the beginning of the 1 min hold time at 50 °C.

Case	T_{max} (°C)	ramp rate (°C/min)	hold time (min)	Number of gran- ules	t_{onset} (s)		Δt (s)		Df/Di	
					mean	std	mean	std	mean	std
A	90	10	2	163	180	18	29	21	2.30	0.32
B	90	5	2	142	276	34	65	46	2.36	0.33
C	70	5	2	48	274	44	51	34	2.38	0.43
D	68	5	15	41	250	37	98	92	2.35	0.25
E	65	5	15	42	293	122	300	169	2.07	0.49

Table 1: Summary of Experimental conditions and swelling data with sigmoid fits

165 Equation 5 defines the degree of swelling parameter which is used to track the swelling
 166 of an individual granule.

$$S(t) = \frac{D(t) - D_i}{D_f - D_i} \quad (5)$$

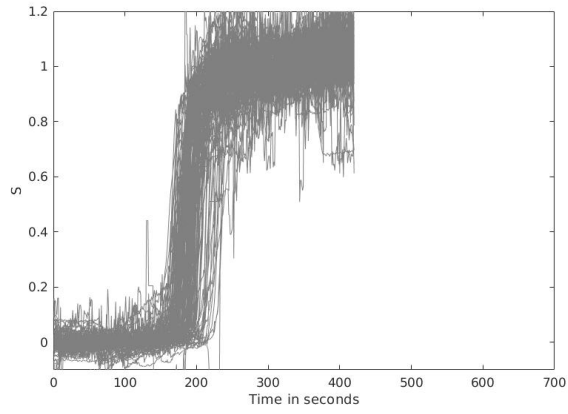
167 Thus, $S(t)$ ranges from 0 to 1, where 0 corresponds to no swelling and 1 corresponds to
 168 complete swelling. To obtain the dimensionless variable S as function of time for each
 169 granule, D_i and D_f obtained from the sigmoid fitting are used. Thus one can obtain cloud
 170 plots of the non-dimensional diameter evolution for each of the experimental cases shown
 171 in figure 1a. The noise observed in the plots of dimensionless variable S is the direct result

172 of noise in the diameter of granule estimated through image processing (Deslandes et al.,
173 2019).

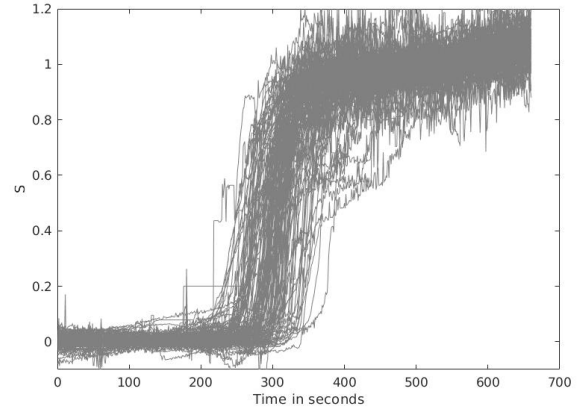
174 From the figure 4 and table 1 it can be concluded that for a given temperature evolution
175 all granules do not begin to swell at the same time. In fact, there is a latency time or delay
176 in onset time involved in the process. The value of this latency time decreases with increase
177 in temperature and varies from granule to granule as seen from the cloud plots in figure 4.
178 Latency time does not depend on the diameter of the granules (Deslandes et al., 2019) and
179 it approximately follows an exponential distribution at a constant temperature as seen in
180 figure 3. It is also observed from figure 4 that granules with high latency time swell less
181 rapidly than the ones with low latency times.

182 Granule diameter reaches a constant value given sufficient time and temperature. In-
183 dividual granule characteristics and temperature profile determine the magnitude of time
184 required to achieve this constant value. The ratio of the final diameter to the initial diameter
185 or simply known as the ratio of swelling (D_f/D_i) varies from granule to granule. This is
186 also reported by Deslandes et al. (2019). The mean ratio of swelling practically is almost
187 independent of the temperature history and initial diameter. This is in accordance with
188 mechanistic models (e.g. (Desam et al., 2020; Briffaz et al., 2014; Watanabe et al., 2001,
189 2007)) in which the final state corresponds to an equilibrium in which the water demand
190 reaches zero. We also did not observe any significant correlation between latency times and
191 swelling ratio(D_f/D_i) based on our data. From table 1 for temperatures above 68 °C we
192 have nearly constant ratio of swelling around 2.35 but for lower temperature of 65°C, the
193 ratio decreases suggesting partial swelling. However, as mentioned in industrial process the
194 temperature used is higher to ensure complete swelling state i.e. swelling ratio of 2.35 in
195 this case. As reported by Deslandes et al. (2019) the ratio of swelling approximately follows
196 a truncated normal distribution.

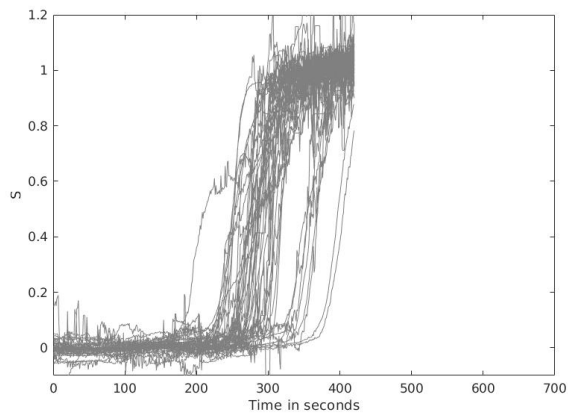
197 These observations were used to develop a novel model that captures most of the essential
198 features, which is discussed in detail in the next section.



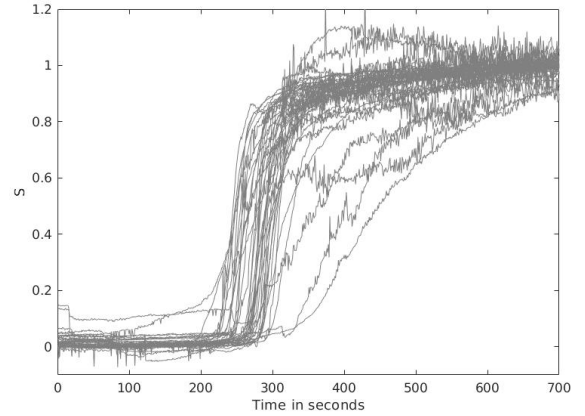
(a) Case A



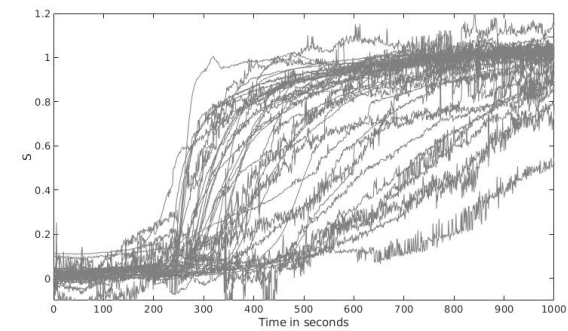
(b) Case B



(c) Case C



(d) Case D



(e) Case E

Figure 4: Non dimensional diameter evolution

199 **4. Model Formulation and Results**

200 *4.1. Kinetic model development*

201 As discussed in the previous section we observed that most granules do not swell at
 202 60 °C even after 1 hour, so we set the minimum temperature of swelling at $T_{min} = 60$ °C
 203 (i.e. below 60 °C there is no swelling of granules). Based on the microscopic images we
 204 observed that each granule has a variable time delay in the onset of swelling which decreases
 205 with increase in temperature. To mathematical formulate the same, let at any instant the
 206 additional fraction (denoted by dF) of granules beginning to swell in next time unit be
 207 proportional to the fraction of granules that did not begin to swell yet (denoted by $1 - F$).
 208 In equation form it can be expressed as

$$dF = \frac{(1 - F)}{\tau} dt \quad (6)$$

209

$$\ln(1 - F) = - \int_0^{t_{onset}} \frac{dt}{\tau} \quad (7)$$

210 Integrating the above requires the knowledge about the characteristic latency time τ which
 211 depends on temperature T. When temperature is constant

$$F = 1 - \exp\left(\frac{-t_{onset}}{\tau}\right). \quad (8)$$

212 Hence in this mathematical formulation we have cumulative density function vs latency
 213 time following the exponential function as was observed in figure 3.

214 We propose that the characteristic latency time in function of temperature follows:

$$\tau = \max\left(0, \left(\frac{T_{ref} - T_{min}}{T - T_{min}}\right)\right) \tau_{ref} \quad (9)$$

215 where T_{ref} is arbitrary fixed at $T_{ref} = 62^\circ C$ and $T_{min} = 60^\circ C$ as indicated previously.

216 Since there is variability of swelling onset between granules, we introduce a parameter
 217 called "difficulty of swelling" parameter $\alpha \in [0, 1]$. For a granule, α is selected at random
 218 from uniform distribution. Thus during the ramp step of the heat treatment for a granule

219 whose difficulty of swelling is α , t_{onset} is given by equation 10.

$$\ln(1 - \alpha) = - \int_0^{t_{onset}} \frac{dt}{\tau} = - \int_0^{t_{onset}} \frac{1}{\tau_{ref}} \max \left(0, \left(\frac{T - T_{min}}{T_{ref} - T_{min}} \right) \right) dt \quad (10)$$

220 During the temperature ramp $T = T_{min} + \beta \times t$, where β is the ramp rate ($^{\circ}C s^{-1}$). Solving
221 equation 10 results in

$$t_{onset} - t_{min} = \left(\frac{-2\ln(1 - \alpha)(T_{ref} - T_{min})\tau_{ref}}{\beta} \right)^{1/2} \quad (11)$$

222 where t_{min} is the time at which $T = T_{min} = 60^{\circ}C$.

223 Once the granule began to swell ($t > t_{onset}$), its diameter increases. A first-order reaction
224 rate is assumed inspired from Kubota et al. (1979), Lund and Lorenz (1984) and Okechukwu
225 and Rao (1995).

$$\frac{dS}{dt} = K(1 - S) \quad (12)$$

226 It is assumed the reaction does not proceed below the cut off temperature T_{min} similar to
227 the previous work by Plana-Fattori et al. (2016).

228 Kinetics for swelling also did speed up as temperature increased. Hence we propose the
229 following equation 13:

$$K = K_{ref}(1 - \alpha)^{0.5} \left(\frac{T - T_{min}}{T_{ref} - T_{min}} \right)^2 \quad (13)$$

230 where K_{ref} is the rate constant at T_{ref} for a granule which has no difficulty to swell ($\alpha = 0$).

231 Thus now one can solve for S of a granule given the temperature profile. Moreover from
232 Deslandes et al. (2019) we know that D_0 and D_{final}/D_0 follow normal distribution.

233 4.2. Calibration of model parameters and model predictions

234 Identification of swelling parameters τ_{ref} and K_{ref} was carried out using the S_{50} of the
235 data obtained from Case A described in table 1 and figure 4. Note that for a median granule
236 by definition the value of α is 0.5. Non-linear fitting of predicted by the model S_{50} with
237 the experimental S_{50} using “fitnlm” function of MATLAB (2018) for the Case A resulted
238 in values $\tau_{ref} = 190$ s and $K_0 = 0.0023$ s⁻¹. This means the median latency time at the

239 reference temperature of 62 °C is 132 seconds i.e. nearly 2 minutes.

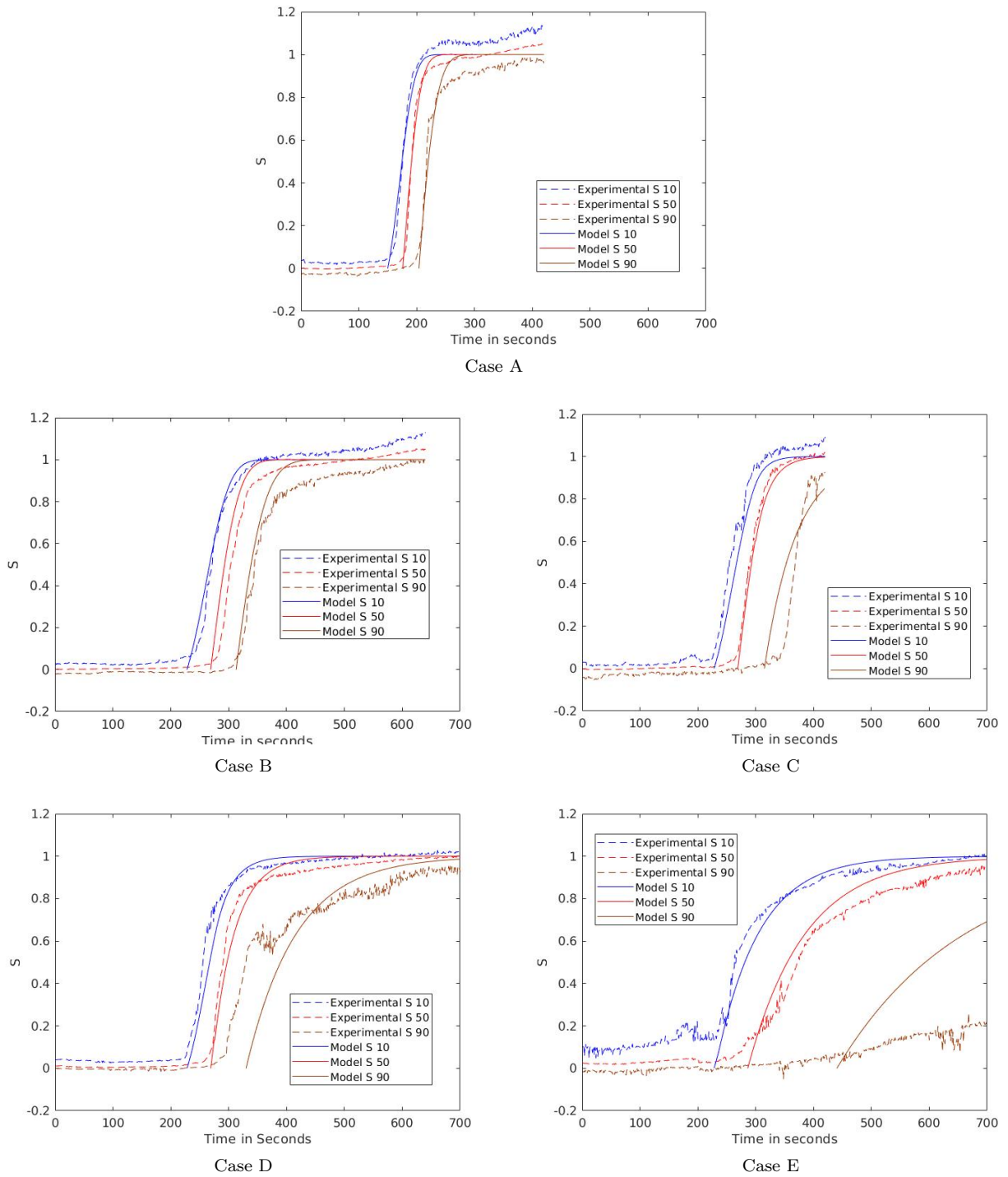


Figure 5: Model prediction of non dimensional diameter evolution

240 Thus now we have a calibrated model. Therefore S_{10} , S_{50} and S_{90} for all the cases can be
 241 predicted and compared with the experimental results. Note that the values of alpha for S_{10}
 242 and S_{90} are 0.1 and 0.9 respectively as previously explained. In the figure 5 the predictions
 243 of S_{10} , S_{50} and S_{90} are shown with respect to the experimental data.

244 It should be noted that due to the noise in the measurement and the value of D_i derived
 245 from fitting the sigmoid curve we have S not beginning exactly at 0 for all the granules at the
 246 initial time points. We see the increase in the dispersion between S_{90} and S_{10} progressively
 247 from cases A to E. These observations are in-line with the model assumptions that rate
 248 constant increase with temperature and latency time decreases with temperature. From the
 249 plots in figure 5, we observe that model predictions overall are close approximations of the
 250 experimental data. The discrepancy for S_{90} in case of D and E could be due to the limited
 251 number of observed granules in this case.

252 4.3. Monte Carlo Simulation and results

253 Now that sufficient confidence has been established in the kinetic model, we can per-
 254 form Monte Carlo simulations and predict the population D_{10} , D_{50} and D_{90} evolution. The
 255 following parameters listed here were used for the simulation

$$256 \quad T_{ref} = 62^\circ C, T_{min} = 60^\circ C,$$

$$257 \quad \tau_{ref} = 190s, K_{ref} = 0.0023s^{-1}, \text{ number of granules } I = 1000,$$

$$258 \quad D_i \subset \mathcal{N}(14.77\mu m, 4.44\mu m), D_f/D_i \subset \mathcal{N}(2.34, 0.33),$$

259 The distributions of D_i and D_f/D_i were calculated from the pool experimental data of
 260 cases A to D. Case E was not considered as we see complete swelling did not always occur in
 261 this case. For granule initial diameter the normal distribution was used with truncated tails
 262 with minimum diameter as $0.25 \times$ mean diameter and maximum value $3 \times$ mean diameter.
 263 The ramp rates and hold times were feed into the simulation as per the individual cases as
 264 tabulated in table 1. A MATLAB script was written to execute the model, 4th order Range
 265 Kutta method was used for integration.

266 It can be observed in figure 6 that the model predictions are close to the experimental data
 267 and the model sufficiently captures the nuances of the process. The slope at the midpoint

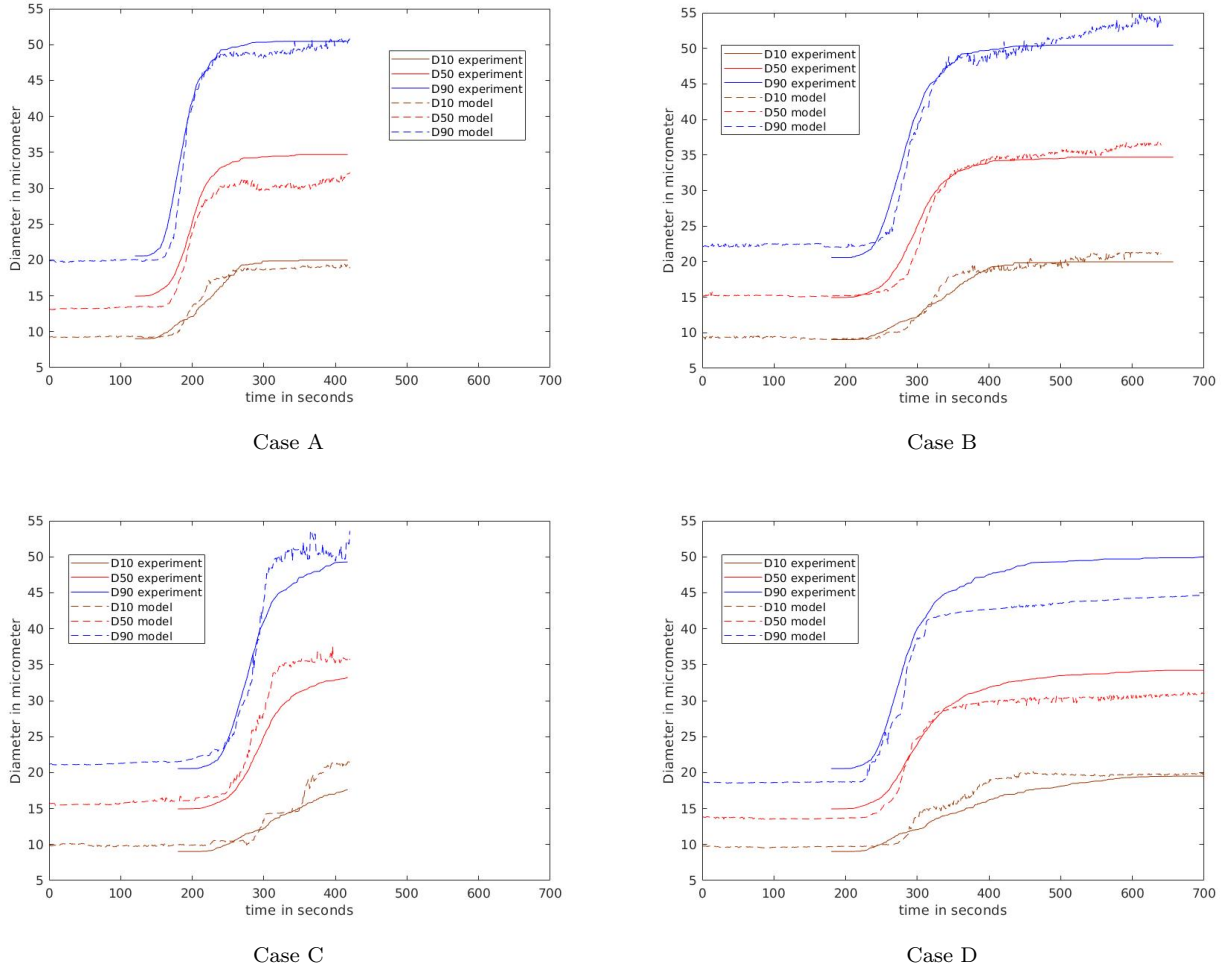
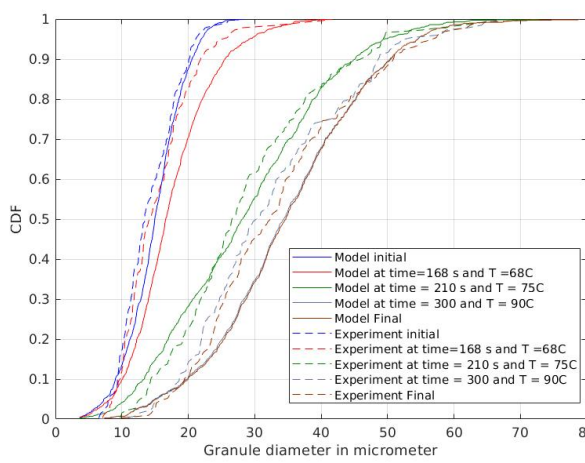


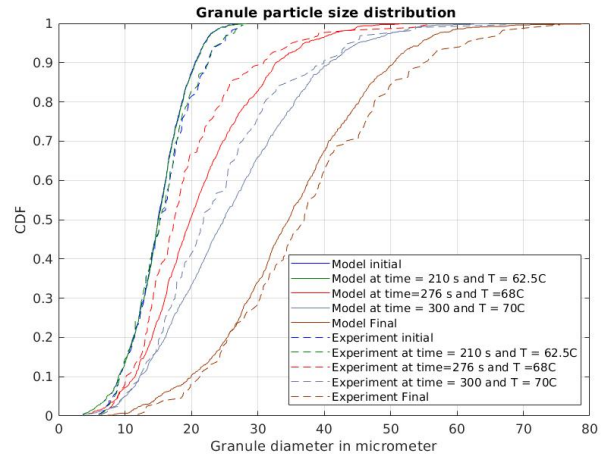
Figure 6: Model prediction of diameter evolution

268 of granule swelling in case A is twice compared to the same in case B. The rate of swelling
 269 is slower progressively with D_{50} and D_{10} compared to D_{90} and this is more pronounced in
 270 the lower temperature cases C and D. The deviation in case D can be attributed to the
 271 lower sample size and higher dispersion at lower temperatures. The latency time is lower for
 272 the higher ramp rate case A compared to the rest of the cases. Finally, both in the model
 273 and the experimental data the dispersion in size is higher after swelling compared to initial
 274 population.

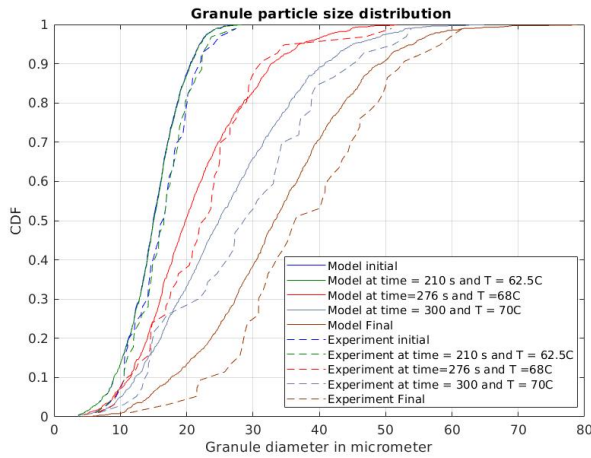
275 Figure 7 presents the cumulative particle size distribution evolution at different time
 276 points as the starch granule swelling proceeds. The dashed curves and continuous are the



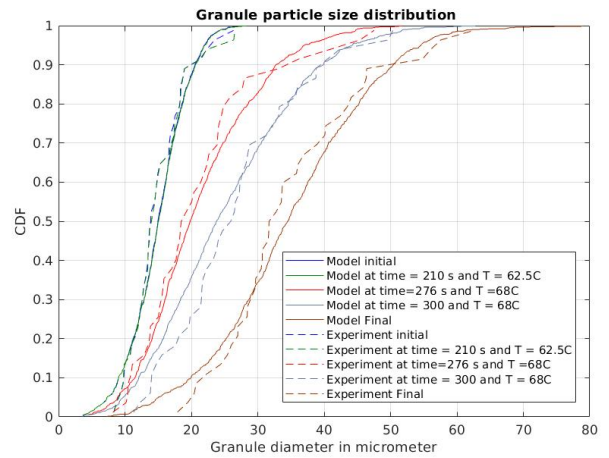
Particle size evolution with time Case A



Particle size evolution with time Case B



Particle size evolution with time Case C



Particle size evolution with time Case D

Figure 7: Cumulative particle size distribution of different cases at different times and temperatures

277 experimentally observed and model predicted particle size distribution respectively. For
 278 both the simulation and experiment the curve at 68 °C in case A is much closer to the initial
 279 one compared to the same temperature in case B. The difference can be attributed to the
 280 difference in latency times (median of 134 seconds vs 197 seconds). This means that not
 281 only temperature is important but also the temperature history together dictate the swelling
 282 of the starch granules. The relative good agreement between predicted and measured size
 283 distributions at intermediate starch swelling for different temperature evolution validate the
 284 applicability of the model.

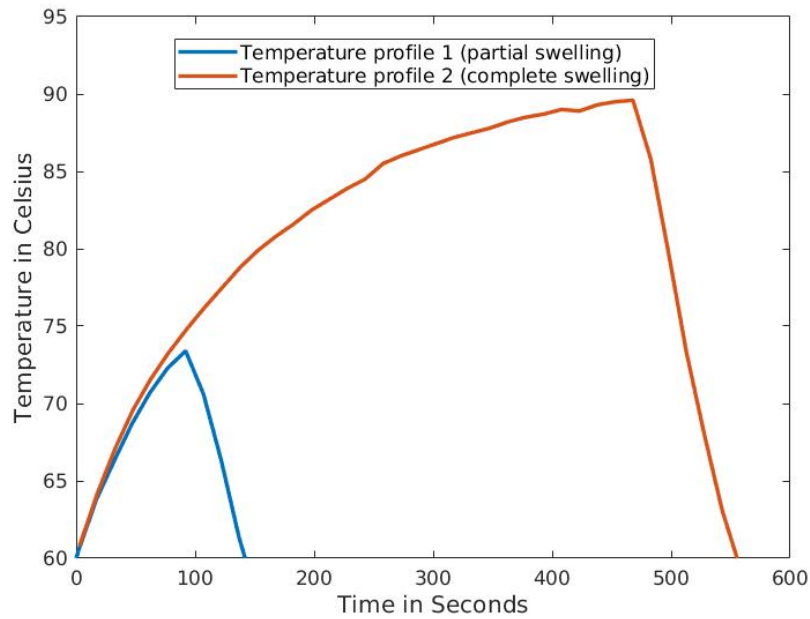
285 *4.4. Model application and validation*

286 In this section we make predictions using the developed model for the population swelling
287 of the same starch using a completely different setup. Plana-Fattori et al. (2016) observed
288 the volume size distributions of starch suspensions after different time-temperature histories
289 using Malvern Mastersizer. The thermal treatment consisted of a series of three water baths,
290 First the sample was immersed in a 50° C water bath until equilibrium was reached, then
291 it was immersed into a water bath maintained at 92° C. After specified “heating time” the
292 sample was shifted to the third water bath maintained at 4° C. All this while the bulk
293 temperature of the sample was measured and noted at regular time intervals of 15 seconds.

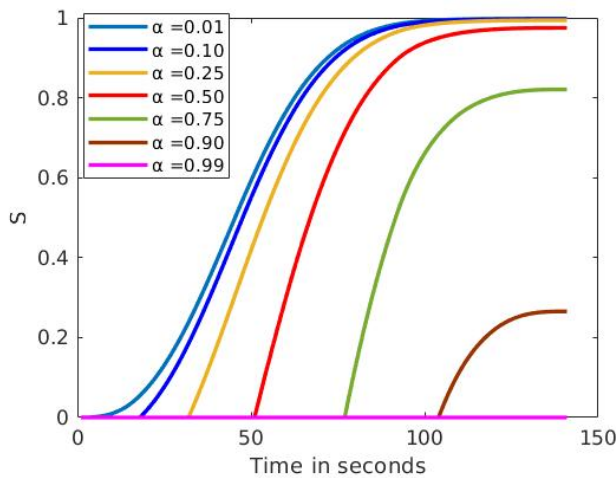
294 For the sake of simplicity we only consider two cases with maximum temperature of 73°
295 C and 92° C respectively (figure 8a). For simulation we only need the bulk temperature
296 profiles above the cut off temperature of 60 ° C. One should note that swelling can go on
297 even during the cooling step as long as the temperature is above 60° C.

298 Monte Carlo simulations using the same parameters mentioned in section 4.3 were per-
299 formed. The difficulty of swelling parameter (α) and the maximum swelling ratio (D_f/D_i)
300 are first randomly chosen for each of 100,000 granules. Then the onset times are calculated
301 according to equation (10) using piece-wise linear interpolation of the experimental temper-
302 ature evolution. The swelling degree (S) evolution are then calculated. The results of such
303 simulations are shown in figure 8b for the first case. Note that because of the decreasing
304 temperature after about 90 s in the first case ($T_{max}=73$ ° C) the rate at which the gran-
305 ules swell decreases in figure 8b. This phenomenon is more evident for α between 0.75 and
306 0.99. Thus some of the granules are in a frozen state of partial swelling in line with the
307 interpretations of Plana-Fattori et al. (2016) in this case.

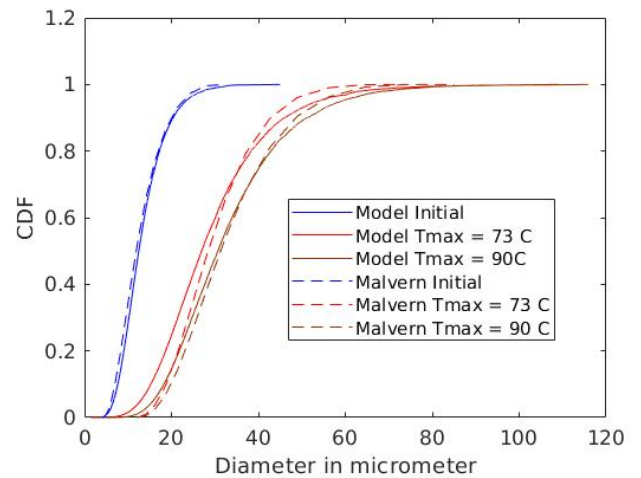
308 From the diameters of the 1000 granules at the end of the heat treatment for both the
309 cases, the volume size distributions were computed to be compared with results from Malvern
310 Mastersizer assuming spherical particles. Initial diameters from the Malvern Mastersizer
311 were used to perform the simulation. The experimental values and model predictions are
312 overlaid in figure 8c. Overall a fairly good prediction is obtained by the model. However,
313 there is discrepancy at lower particle sizes for $T_{max}=73$ °C. Considering the differences in the



(a) Bulk Temperature profiles recorded for heating times of 2 minutes and 8 minutes (Courtesy of Plana-Fattori et al. (2016))



(b) Non-dimensional diameter evolution temperature profile 1



(c) Cumulative volume distribution

Figure 8

314 measuring techniques (microscopy for model fitting, light diffraction for Malvern) and various
 315 experimental and model assumptions (spherical particles, temperature uniform across the
 316 sample, $T_{min} = 60 \text{ } ^\circ \text{C}$) the performance of the model on a whole is good, notably to predict
 317 the size distribution of partially gelatinized starch which is of practical interest (Hickman
 318 et al., 2008).

319 4.5. Possible explanation of variability and model limitations

320 The presented empirical model is based on individual granules observation and does not
321 explain why different granules submitted to the same temperature evolution begin to swell at
322 different instants (t_{onset}) and with different swelling duration (Δt). Literature suggests that
323 various mechanisms are involved during starch swelling : melting of crystallites, moisture
324 sorption, water diffusion, fusion of amylose/lipid complexes, leaching of amylose into the
325 continuous phase, rupture of the granular structure (Briffaz et al., 2013, 2014; Chapwanya
326 and Misra, 2015; Ozturk and Takhar, 2018). The three last phenomena do not occur in our
327 case as waxy cross-linked maize starch was used for this work. In addition since we consider
328 a very dilute system, there is no water availability limitation as discussed by Fukuoka et al.
329 (2002).

330 Debet and Gidley (2006) identified three classes of starch granule swelling: (i) rapid
331 swelling, (ii) slow swelling, (iii) limited swelling. For waxy maize starch there is no inter-
332 action between amylose, surface proteins and lipids and therefore rapid one-step swelling is
333 observed. For other types of starch, the maximal swelling ratio can be function of the highest
334 temperature reached. Indeed after a first swelling step (typically between 60 and 70 °C), a
335 second step (typically between 80 and 100 °C) is observed, related to amylose/lipid/protein
336 interaction for other types of starches (Briffaz et al., 2013). In our case, D_f/D_i was found
337 to be independent on the maximal temperature (for $T_{max} > 65^\circ C$).

338 Melting of crystallites and moisture sorption can be affected by different parameters
339 which can vary between granules such as crystallinity, branching of amylopectin, degree
340 of cross linking, etc. (Debet and Gidley, 2006). This can explain variability in t_{onset} and
341 Δt which was taken into account by a random parameter α (difficulty of swelling). One
342 could expect that the 'difficulty of swelling' also influences the swelling ratio D_f/D_i , but no
343 correlation was observed in our case between D_f/D_i and t_{onset} (p value $\sim 0.95 \gg 0.05$).

344 Diffusion can be assumed as Fickian (based on water concentration gradient), non-Fickian
345 (based on water demand) (Watanabe et al., 2001) or following Flory-Huggins theory (Desam
346 et al., 2018, 2020). Tortuosity can be considered as function of aqueous volume fraction
347 and can vary between granules depending on the amorphous/crystalline shell structure. If

348 water availability is limited due to diffusion, the smallest granules should swell more rapidly.
349 However, this was not observed in our case, there is no correlation between D_i and t_{onset} ,
350 Δt or D_f/D_i . It seems that in our case diffusion is not the limiting factor; different models
351 were tested previously which confirmed that a diffusion based model is not pertinent for this
352 kind of starch (Almeida et al., 2015).

353 To summarize, in our case (waxy cross-linked maize starch) variability in swelling onset
354 and swelling duration could be attributed to the variability between granules in terms of
355 crystallinity/structure, branching of amylopectin, cross linking. This variability comes per-
356 haps from the different positions in the corn, positions on the cob, maturity, intra-granular
357 heterogeneity, etc. These parameters influence the melting of the crystallites and the water
358 diffusion. However, in our case the diffusion seems to not be the limiting phenomenon since
359 the smallest granules do not swell faster than the biggest ones. It could be interesting to
360 introduce variability for water activity curves and tortuosity in mechanistic swelling models
361 such as the one developed by Desam et al. (2020). This approach could help one deter-
362 mine which of these parameters might potentially explain the swelling kinetics variability.
363 For more complex starches (non-waxy or non-cross-linked) the presented model is perhaps
364 not adapted and additional experimental efforts are required because additional phenomena
365 occur.

366 5. Conclusion

367 A novel individual granule scale model was developed to predict the swelling kinetics
368 of modified waxy maize starch granules under heat treatment. The model parameters were
369 calibrated with data from one ramp rate and hold temperature and validated with data from
370 other cases. From the experiments it is shown that there is granule to granule variability
371 not only in terms of ratio of swelling but also in terms of latency to swell when a critical
372 temperature is reached. These phenomena are independent of the diameter of the granules.
373 For practical time scales we can say the swelling reaction does not initiate below 60 °C.
374 The latency time is random with a characteristic time constant decreasing as temperature is
375 increased. Also the kinetics of the reaction is enhanced at higher temperatures. A granule

376 with high latency time is also shown to have slower swelling rate compared to granules with
377 low latency time.

378 The rheology of the suspension results from the hydrodynamic interactions and collisions
379 between the granules which is a function of the volume fraction of granules and granule PSD.
380 To design, control, scale up and operate complex processes for liquid food products one needs
381 to leverage simulation techniques such as Computational Fluid Dynamics (fluid flow, heat
382 transfer) and Discrete Element Method (particle evolution and interaction). This granule
383 scale model can represent the commencement of such techniques for multi-scale modelling
384 and simulation of modified starch suspension undergoing thermal treatment.

385 **6. Acknowledgments**

386 This research has been carried out with funding from European Union as part of
387 EU RESEARCH FRAMEWORK PROGRAMME: H2020 / Marie Skłodowska-Curie Ac-
388 tions ITN MATHEGRAM [813202].

389 We acknowledge Giana Almeida-Perré and Gabrielle Moulin (UMR-SayFood) for their sup-
390 port and contributions.

391 **References**

- 392 Almeida, G., Plana-Fattori, A., Moulin, G., Michon, C., and Flick, D. Observing and modeling the evolution
393 of starch granules size distribution. In *6. International Symposium on Delivery of Functionality in Complex*
394 *Food Systems. Physically-Inspired Approaches from the Nanoscale to the Microscale*, 2015.
- 395 Anuntagool, J., Alvarez, G., and Flick, D. Predictive model for viscosity development of modified rice starch
396 suspension under unsteady temperature change. *Journal of Food Engineering*, 209:45–51, 2017.
- 397 Ashogbon, A. O. and Akintayo, E. T. Recent trend in the physical and chemical modification of starches
398 from different botanical sources: A review. *Starch-Stärke*, 66(1-2):41–57, 2014.
- 399 Atwell, W. The terminology and methodology associated with basic starch phenomena. *Cereal Foods World*,
400 33:306–311, 1988.
- 401 Bagley, E. and Christianson, D. Swelling capacity of starch and its relationship to suspension viscosity-effect
402 of cooking time, temperature and concentration. *Journal of Texture Studies*, 13(1):115–126, 1982.
- 403 Bakshi, A. and Singh, R. Kinetics of water diffusion and starch gelatinization during rice parboiling. *Journal*
404 *of Food Science*, 45:1387 – 1392, 1980.

405 Banks, W., Greenwood, C., and Muir, D. Studies on starches of high amylose content. part 17. a review of
406 current concepts. *Starch-Stärke*, 26(9):289–300, 1974.

407 Bertolini, A. C. *Trends in starch applications. Starches: Characterization, Properties, and Applications.*
408 Taylor and Francis Group, LLC, Abingdon, 2010.

409 Biliaderis, C. G. and Prokopowich, D. J. Effect of polyhydroxy compounds on structure formation in waxy
410 maize starch gels: a calorimetric study. *Carbohydrate Polymers*, 23(3):193–202, 1994.

411 Biliaderis, C. Structure and phase transitions of starch in food system. *Food Technol.*, 46:98–109, 1992.

412 Blennow, A., Bay-Smidt, A. M., and Bauer, R. Amylopectin aggregation as a function of starch phos-
413 phate content studied by size exclusion chromatography and on-line refractive index and light scattering.
414 *International Journal of Biological Macromolecules*, 28(5):409–420, 2001.

415 Briffaz, A., Mestres, C., Matencio, F., Pons, B., and Dornier, M. Modelling starch phase transitions and
416 water uptake of rice kernels during cooking. *Journal of Cereal Science*, 58(3):387–392, 2013.

417 Briffaz, A., Bohuon, P., Méot, J.-M., Dornier, M., and Mestres, C. Modelling of water transport and swelling
418 associated with starch gelatinization during rice cooking. *Journal of food engineering*, 121:143–151, 2014.

419 Chang, S.-M. and Liu, L.-C. Retrogradation of rice starches studied by differential scanning calorimetry
420 and influence of sugars, nacl and lipids. *Journal of Food Science*, 56(2):564–566, 1991.

421 Chapwanya, M. and Misra, N. A soft condensed matter approach towards mathematical modelling of mass
422 transport and swelling in food grains. *Journal of Food Engineering*, 145:37–44, 2015.

423 Chen, G., Campanella, O. H., and Purkayastha, S. A dynamic model of crosslinked corn starch granules
424 swelling during thermal processing. *Journal of Food Engineering*, 81(2):500–507, 2007.

425 Choi, S.-G. and Kerr, W. L. Swelling characteristics of native and chemically modified wheat starches as a
426 function of heating temperature and time. *Starch-Stärke*, 56(5):181–189, 2004.

427 Cui, L., Dong, S., Zhang, J., and Liu, P. Starch granule size distribution and morphogenesis in maize ('zea
428 mays' l.) grains with different endosperm types. *Australian Journal of Crop Science*, 8(11):1560–1565,
429 2014.

430 Debet, M. R. and Gidley, M. J. Three classes of starch granule swelling: Influence of surface proteins and
431 lipids. *Carbohydrate Polymers*, 64(3):452–465, 2006.

432 Desam, G. P., Li, J., Chen, G., Campanella, O., and Narsimhan, G. A mechanistic model for swelling
433 kinetics of waxy maize starch suspension. *Journal of Food Engineering*, 222:237–249, 2018.

434 Desam, G. P., Li, J., Chen, G., Campanella, O., and Narsimhan, G. Swelling kinetics of rice and potato
435 starch suspensions. *Journal of Food Process Engineering*, 43(4):e13353, 2020.

436 Deslandes, F., Plana-Fattori, A., Almeida, G., Moulin, G., Doursat, C., and Flick, D. Estimation of
437 individual starch granule swelling under hydro-thermal treatment. *Food Structure*, 22:100125, 2019.

438 Dolan, K. D. and Steffe, J. F. Modeling rheological behavior of gelatinizing starch solutions using mixer

439 viscometry data. *Journal of Texture Studies*, 21(3):265–294, 1990.

440 Doublier, J.-L., Llamas, G., and Le Meur, M. A rheological investigation of cereal starch pastes and gels.
441 effect of pasting procedures. *Carbohydrate Polymers*, 7(4):251–275, 1987.

442 Evans, I. D. and Lips, A. Concentration dependence of the linear elastic behaviour of model microgel
443 dispersions. *Journal of the Chemical Society, Faraday Transactions*, 86(20):3413–3417, 1990.

444 Fredriksson, H., Silverio, J., Andersson, R., Eliasson, A.-C., and Åman, P. The influence of amylose and
445 amylopectin characteristics on gelatinization and retrogradation properties of different starches. *Carbo-*
446 *hydrate polymers*, 35(3-4):119–134, 1998.

447 Fukuoka, M., Ohta, K.-i., and Watanabe, H. Determination of the terminal extent of starch gelatinization
448 in a limited water system by DSC. *Journal of Food Engineering*, 53(1):39–42, 2002.

449 Hickman, B. E., Janaswamy, S., and Yao, Y. Properties of starch subjected to partial gelatinization and
450 β -amylolysis. *Journal of Agricultural and Food Chemistry*, 57(2):666–674, 2008.

451 Hoover, R. Composition, molecular structure, and physicochemical properties of tuber and root starches: a
452 review. *Carbohydrate polymers*, 45(3):253–267, 2001.

453 I’anson, K., Miles, M., Morris, V., Besford, L., Jarvis, D., and Marsh, R. The effects of added sugars on the
454 retrogradation of wheat starch gels. *Journal of Cereal Science*, 11(3):243–248, 1990.

455 Kohyama, K. and Nishinari, K. Effect of soluble sugars on gelatinization and retrogradation of sweet potato
456 starch. *Journal of Agricultural and Food Chemistry*, 39(8):1406–1410, 1991.

457 Kokini, J., Lai, L.-S., and Chedid, L. L. Effect of starch structure on starch rheological properties. *Food*
458 *Technology*, 46:124–139, 1992.

459 Krüger, A., Ferrero, C., and Zaritzky, N. E. Modelling corn starch swelling in batch systems: effect of
460 sucrose and hydrocolloids. *Journal of Food Engineering*, 58(2):125–133, 2003.

461 Kubota, K., Hosokawa, Y., Suzuki, K., and Hosaka, H. Studies on the gelatinization rate of rice and potato
462 starches. *Journal of Food Science*, 44(5):1394–1397, 1979. doi: 10.1111/j.1365-2621.1979.tb06446.x.

463 Lagarrigue, S., Alvarez, G., Cuvelier, G., and Flick, D. Swelling kinetics of waxy maize and maize starches
464 at high temperatures and heating rates. *Carbohydrate Polymers*, 73(1):148–155, 2008.

465 Lund, D. and Lorenz, K. J. Influence of time, temperature, moisture, ingredients, and processing conditions
466 on starch gelatinization. *C R C Critical Reviews in Food Science and Nutrition*, 20(4):249–273, 1984.

467 Malumba, P., Jacquet, N., Delimme, G., Lefebvre, F., and Béra, F. The swelling behaviour of wheat starch
468 granules during isothermal and non-isothermal treatments. *Journal of Food Engineering*, 114(2):199–206,
469 2013.

470 Malumba, P., Doran, L., Danthine, S., Blecker, C., and Béra, F. The effect of heating rates on functional
471 properties of wheat and potato starch-water systems. *LWT*, 88:196–202, 2018.

472 MATLAB. *version 9.4.0.813654 (R2018a)*. The MathWorks Inc., Natick, Massachusetts, 2018.

473 Miles, M. J., Morris, V. J., Orford, P. D., and Ring, S. G. The roles of amylose and amylopectin in the
474 gelation and retrogradation of starch. *Carbohydrate research*, 135(2):271–281, 1985.

475 Nayouf, M., Loisel, C., and Doublier, J. Effect of thermomechanical treatment on the rheological properties
476 of crosslinked waxy corn starch. *Journal of Food Engineering*, 59:209–219, 2003.

477 Okechukwu, P. E. and Rao, M. A. Influence of granule size on viscosity of cornstarch suspension. *Journal*
478 *of Texture Studies*, 26(5):501–516, 1995.

479 Okechukwu, P. E. and Rao, M. A. Kinetics of cowpea starch gelatinization based on granule swelling.
480 *Starch-Stärke*, 48(2):43–47, 1996.

481 Ozturk, O. K. and Takhar, P. S. Water transport in starchy foods: Experimental and mathematical aspects.
482 *Trends in Food Science & Technology*, 78:11–24, 2018.

483 Plana-Fattori, A., Flick, D., Ducept, F., Doursat, C., Michon, C., and Mezdour, S. A deterministic approach
484 for predicting the transformation of starch suspensions in tubular heat exchangers. *Journal of Food*
485 *Engineering*, 171:28–36, 2016.

486 Ratnayake, W. S. and Jackson, D. S. Starch gelatinization. *Advances in Food and Nutrition Research*, 55:
487 221–268, 2008.

488 Singh, J., Kaur, L., and McCarthy, O. Factors influencing the physico-chemical, morphological, thermal
489 and rheological properties of some chemically modified starches for food applications—a review. *Food*
490 *Hydrocolloids*, 21(1):1–22, 2007.

491 Slade, L. and Levine, H. A food polymer science approach to structure-property relationships in aqueous
492 food systems: Non-equilibrium behavior of carbohydrate-water systems. In *Water Relationships in Foods*,
493 pages 29–101. 1991.

494 Slade, L. and Levine, H. Glass transitions and water-food structure interactions. In *Advances in Food and*
495 *Nutrition Research*, volume 38, pages 103–269. 1995.

496 Srichuwong, S., Sunarti, T. C., Mishima, T., Isono, N., and Hisamatsu, M. Starches from different botanical
497 sources ii: Contribution of starch structure to swelling and pasting properties. *Carbohydrate Polymers*,
498 62(1):25–34, 2005.

499 Steeneken, P. Rheological properties of aqueous suspensions of swollen starch granules. *Carbohydrate*
500 *Polymers*, 11(1):23–42, 1989.

501 Suzuki, U., Kubota, K., Omichi, M., and Hosaka, H. Kinetic studies on cooking of rice. *Journal of Food*
502 *Science*, 41:1180 – 1183, 1976.

503 Szczesniak, A. S. Classification of textural characteristics a. *Journal of Food Science*, 28(4):385–389, 1963.

504 Tattiyakul, J. and Rao, M. A. Rheological behavior of cross-linked waxy maize starch dispersions during
505 and after heating. *Carbohydrate Polymers*, 43(3):215–222, 2000.

506 Thomas, D. and Atwell, W. Eagan press handbook series: Starches. st. paul, minnesota, usa eagan press.,

507 1999.

508 Visser, R. G. F., Suurs, L. C. J. M., Steeneken, P. A. M., and Jacobsen, E. Some physicochemical properties
509 of amylose-free potato starch. *Starch-Stärke*, 49(11):443–448, 1997.

510 Watanabe, H., Fukuoka, M., Tomiya, A., and Mihori, T. A new non-fickian diffusion model for water
511 migration in starchy food during cooking. *Journal of Food Engineering*, 49(1):1–6, 2001.

512 Watanabe, H., Yahata, Y., Fukuoka, M., Sakiyama, T., and Mihori, T. The thermodynamic basis for the
513 relative water demand model that describes non-fickian water diffusion in starchy foods. *Journal of food
514 engineering*, 83(2):130–135, 2007.

515 Wood, F. W. Psychophysical studies on the consistency of liquid foods. *Rheology and Texture of Food Stuffs*,
516 *SCI Monograph*, 27:40–49, 1968.